A New Image Blood Pressure Sensor Based on PPG, RRT, BPTT, and Harmonic Balancing

Sheng-Chieh Huang, Pei-Hsuan Hung, Chung-Hung Hong, and Hui-Min Wang

***Abstract*— A new blood pressure (BP) sensor, also named sphygmomanometer, is developed in this paper for estimating BPs accurately from fingertips. The hardware of the sensor is a low-cost optical CMOS imaging device for detecting photoplethysmography (PPG) signals at fingertips. Therefore, the sensor neither needs to contact human skin nor pressurize it for accurate BP predictions. To calculate BPs based on captured PPG signals, the modified radial resonance theory is applied to develop a new BP transport theory (BPTT), and then composes a computation algorithm for implementing BPTT in a typical smart phone with limited computation load required. The algorithm is successfully implemented in a typical smart phone with minimum computation load and equipped with an efficient calibration process. An experiment is conducted to evaluate the performance of the designed BP-sensing techniques. The resulted data clearly show that the difference between the systolic BPs (SBPs) sensed by the propose sensor and a validated cumbersome instrument is 1.37 mmHg, while for diastolic BPs (DBPs) is −1.40 mmHg. The afore-reported accuracy is well below those required by the Association for the Advancement of Medical Instrumentation, which are ±5 and 8 mmHg, respectively, for SBPs and DBPs.**

***Index Terms*— Photoplethysmography (PPG), blood pressure sensor, radial resonance theory, sphygmomanometer, blood pressure transport theory.**

I. Introduction

MANY people suffer chronic cardiovascular diseases. To cope with these diseases, it is desired to develop simple, ubiquitous and non-invasive sensors to obtain physiological information for early and primitive diagnosis. Among varied physiological signals, like heart rate, glucose, ECG, EEG and blood pressures (BPs), the blood pressure is one of the most important informations for doctors to conduct diagnosis, however, it is very difficult to detect as compared to all the other biological signals. For accurate blood pressures, one can adopt an invasive approach to obtain the correct blood pressure via clinical operations, but it is inconvenient and dangerous to health stability of a human body. Traditional non-invasive blood-measuring system includes an inflatable cuff, signal processing unit and controller, along with two calculation methods: auscultation and oscillation [17]. Since the whole system is cumbersome, recently, new methods have been under development for next-generation "cuffless" sensors, like radio-frequency (RF) detective methods, photoplethysmography (PPG) method, etc [1]–[5]. On the other hand, physical sensor hardware is also one of popular topics along with the aforementioned detection methods [6]. In this study, a novel non-invasive, non-pressurized method based PPG signals is developed to compute the blood pressures via the modified radial resonance theory [7]–[12] and a newly-developed blood pressure transport theory based on the digital images captured by a CMOS camera that can be incorporated into a smart phone. Since the whole measurement is executed in a non-invasive fashion, performable by the CMOS camera in smart phones and needing only a short period of time, the blood-pressure sensing methodology proposed herein would bring benefits of continuous monitoring and comfort to the patients with hypertension problems.

The organization of the remainder of this paper is as follows. In Section II, the modified radial resonance theory and device are introduced. In Section III experimental results are discussed. In Section IV, conclusions are given.

Manuscript received March 10, 2014; revised May 28, 2014; accepted May 28, 2014. Date of publication June 9, 2014; date of current version August 29, 2014. The associate editor coordinating the review of this paper and approving it for publication was Prof. Paul C.-P. Chao.

The authors are with the Department of Electrical and Computer Engineering, National Chiao-Tung University, Hsinchu 30010, Taiwan (e-mail: schuang@cn.nctu.edu.tw; wwwxxx12@yahoo.com.tw; hongchunghung@gmail.com; marcel.wang@gmail.com).

Color versions of one or more of the figures in this paper are available online at http://ieeexplore.ieee.org.

Digital Object Identifier 10.1109/JSEN.2014.2329676

II. Method and Theory

A. Modified Radial Resonance Theory

According to radial resonance theory (RRT) [7]–[11], a human arterial system can be regarded as a cylindrical elastic tube network with adherent fluid [7]. Excited by the heart, the elastic blood vessel wall is then in periodic vibration with resulted radial dilations, further exhibiting propagation of pressure wave from one end of the artery to another. In this pressure wave propagation, the diameter at a given arterial location dilates periodically in accordance with pulsation, while the energy coming from heart is stored in the manner of elastic energy and passed along by arteries.

Equations of motion prescribing pressure wave propagation of arterial wall are first derived for further accurate blood pressure predictions. The derivation essentially follows those in [7]. The external pressure of the arterial vessel tube is denoted by P_{e}, while the internal fluid pressure is P. In the static condition, the fluid pressure is P_{o}, the inner radius of the cylinder is r_{o}, and the thickness of the wall is h_{o}. The excitation on the arterial tube is assumed of impulses at heart, at one end of tube. Z denotes the longitudinal coordinate along the artery, while $r(\mathrm{Z},t)$ captures the radial dilation of the arterial tube. A small element that is part of the tube's i-th segment at position Z is considered, which is of an axial length $\Delta\mathrm{Z}$. An element with circumferential angle $d\theta$

1530-437X © 2014 IEEE. Personal use is permitted, but republication/redistribution requires IEEE permission.
See http://www.ieee.org/publications_standards/publications/rights/index.html for more information.

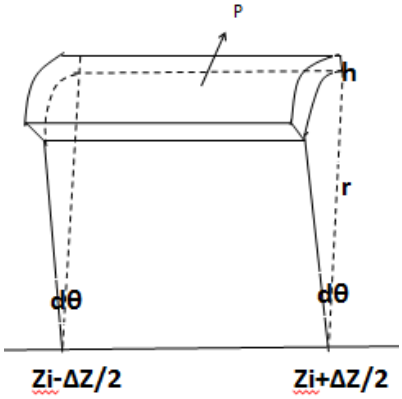

Fig. 1. A segmented small element of the arterial wall [6].

is illustrated by Fig.1. All the forces and moments acting on the element are derived by the following steps of analysis.

1) The total restoring force, F_N, exerted from the deformation of the small element and acting in the radial direction can be formulated as

$$F_N = -E_N \frac{\Delta r}{r_0} \Delta Z_r d\theta, \tag{1}$$

where E_N is the sum of the Young's modules of wall material in radial and circumferential directions.

2) The total shear force, F_S, acting on the two Z-planes, which tends to restore the element in Fig. 1 back to the orientation parallel to Z-axis can be expressed by

$$F_S = (E_{rZ} \frac{dr}{dz} hrd\theta)_{Z_i + \frac{\Delta Z}{2}} - (E_{rZ} \frac{dr}{dz} hrd\theta)_{Z_i - \frac{\Delta Z}{2}}, \tag{2}$$

where E_{rZ} is the shear modulus of the wall material of the arterial vessel tube.

3) The resistance force in the radial direction, F_f, induced by the viscosity between arterial wall and adherent blood fluid can be derived by

$$F_f = -R_i \Delta Z r d\theta \frac{dr}{dt}, \tag{3}$$

where R_i is the viscosity.

4) The momentum of the element, M, in the radial direction is

$$M = d\theta \mu \Delta Z r \frac{dr}{dt}, \tag{4}$$

where μ is an equivalent density combining arterial tube material and adherent blood fluid.

Based on the fundamental Newton's second law, the momentum in Eq. (4) equals to sum of forces in Eqs. (1)–(3), yielding a balance in the radial direction,

$$\begin{aligned} d\theta \mu \Delta Z \frac{d}{dt}(r \frac{dr}{dt}) &= d\theta \left\{ -E_N \frac{\Delta r}{r_0} \Delta Z_r + (E_{rZ} \frac{dr}{dz} h_r)_{Z_i + \frac{\Delta Z}{2}} \right. \\ &\left. -(E_{rZ} \frac{dr}{dz} h_r)_{Z_i - \frac{\Delta Z}{2}} - R_i \Delta Z r \frac{dr}{dt} \right\}. \end{aligned} \tag{5}$$

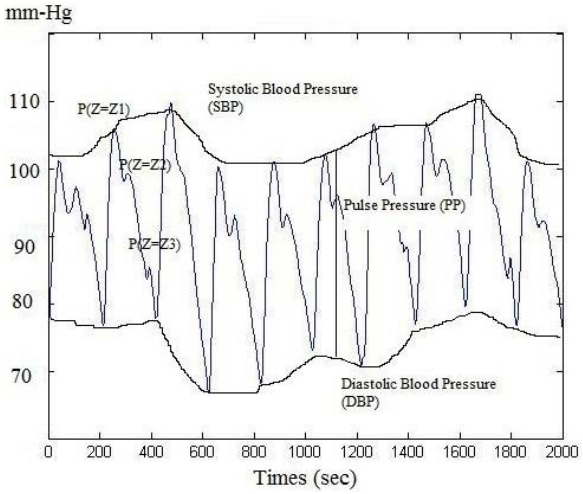

Fig. 2. Typical blood pressure waveforms.

Canceling $d\theta$'s at both sides of Eq. (5) and further manipulating, one can arrive at the governing equation below by letting ΔZ approaching dZ,

$$\mu \frac{d^2 P}{dt^2} + R_i \frac{dP}{dt} + \frac{E_N}{r_0} P = E_{rZ} h \frac{d^2 P}{dt^2}. \tag{6}$$

The above equation governs the propagating blood pressure wave and is next due to solve. The solution process can be started by expressing $P(z,t)$ by decomposing its spatial and temporal dependences in n-terms series for approximation, i.e.,

$$P(z,t) = \sum_{n=0}^{N} P_n(z) \cos(\omega_n t). \tag{7}$$

where ω_0 is the fundamental vibratory frequency of the arterial tube, while ω_n's are multiples of ω_0, the harmonics associate with which are induced as the radial vibratory dilation propagates from heart to their ends.

B. Blood Pressure Transport Theory (BPTT)

Typical blood waveforms are similar to the actual measurements as shown in Fig. 2. They can be seen as a periodic signal in one frequency as prescribed by Eq. (7), while its amplitudes varying with time evolves in another slower frequency [7]–[11]. The upper and lower envelopes of signal amplitude evolution as seen in Fig. 2 are actually commonly-known systolic blood pressure (SBP) and diastolic blood pressure (DBP) waveforms, respectively. The difference between SBP and DBP waveforms is named "pulse pressure" (PP). The oscillating frequency of the pulse pressure results from heart beats, therefore in accordance with heart rate (HR) and following Eq. (7), while those of SBP and DBP enveloping waveforms are associated with other-order harmonics resulted from vibrations reflected from blood vessel extremities (the ends of cardiovascular system at limbs; arms and legs) and respirations, thus including other-order harmonics and respiratory rate (RR). Based on the characteristics seen in the waveforms shown in Fig. 2 – periodicity and varying amplitudes, the signal can be regarded as a periodic signal

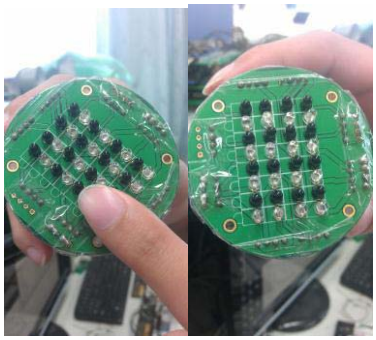

Fig. 3. Finger-tip PPG signals measured by a custom-made interposed array of IR-LEDs and PDs.

Fig. 4. Finger-tip PPGs measured by a CMOS camera in a smart phone.

in HR with its amplitude modulated between SBP and DBP in distinct-order harmonics and/or RR, i.e., the so-called "beating" phenomenon. Therefore, the method often used for prescribing amplitude modulation of propagating radio frequency signals [18] can be adopted herein to describe the transport of the blood pressure waveforms in Fig. 2 from one end of the arterial tube to another. Following this recommended method, at a given instant the blood pressures obeying Eqs. (6), (7) at different locations of the arterial tube, z_{i} and $z_{\mathrm{i}+1}$, satisfies

$$P(z_{i+1}, t) = P(z_i, t)[a\cos(\omega_b t) + (1 - a)], \tag{8}$$

where a is the strength coefficient of amplitude modulation between systole and diastole, which is from 0 to 0.5, and ω_b is the frequency of higher-order and/or HR harmonics riding on baseline oscillation due to heart beat $P(z_{\mathrm{i}}, t)$. The subscript b stands for beating. Based on Eq. (8), one is able to predict BP waveform including SBPs and DBPs at any given location of the arterial vessel network based on the actual measurement at any other given arterial location. This newly developed theory in Eq. (8) is named "blood pressure transport theory (BPTT)," which would be realized by an algorithm in subsection II.D and further confirmed by experiment in section III.

C. PPG Sensors

The application of BPTT is practiced in this study by the case that PPG signals are sampled at fingertip by varied sensors, while the computation algorithm developed later based on BPTT would be able to predict BPs at the artery outlet from the heart (doctors' favorable) and the upper arm (traditional BP measurement device) based on the PPGs sensed at fingertip. The sensor hardware could be an interposed array of infrared light emitter diodes (IR-LEDs) and photo detectors (PDs) or the module of an LED or a CMOS camera [16] integrated in a typical smart phone, as shown in Figs. 3 and 4, respectively. The light emitted by LEDs reaches skin, penetrates to arteries beneath, and then reflects. The reflected light is finally detected by the sensor as PPG signals. Note that along varied traces, the light intensities are all attenuated by absorptions through skins, muscles, bones and blood. Due to relative stillness of skins, muscles and bones to blood vessel, any temporal variation embedded in the reflected light intensity waveform detected by the sensor is caused by dynamic blood vessel dilation. Considering the fact that as the arterial vessel dilates, it absorbs much light due to a larger volume, thus the PPG signal detected by sensor can be prescribed by

$$I'(t) = I - k\pi r(t)^2, \tag{9}$$

where I' is the intensity of the light sensed by the sensor; I is the intensity of the light without considering the absorption due to dynamic arterial vessel dilation; $r(t)$ is the radius of the artery varying with dynamic dilation; k is the modulus of the absorbed energy per unit cross section of the area of the arterial tube. In Eq. (9), the ac component of I' is due to reflection of dynamic artery dilation, since blood vessel deforms as opposed to other relative still bio-structure and materials. The relationship between $r(t)$ and blood pressure (BP), $P(t)$, could be expressed as

$$\pi r(t)^2 = C_A P(t) + c, \tag{10}$$

where C_{A} is the compliance of vessel size to blood pressure; c is a fitting constant. Substituting Eq. (10) into (9) yields

$$I'(t) = -kC_A P(t) + I_0, \tag{11}$$

where I_0 accounts for integral constant (dc) effects. Based on the linear relation between BP and PPG signals in Eq. (11), the PPG signals are ready for extracting BPs with appropriate calibrations.

D. Computation Algorithm for BPTT

With PPG sensors ready, the proposed BPTT is applied to develop a computation algorithm to estimate DBPs and SBPs at one location of the arterial tube based on BP waveforms elsewhere. This task is regarded very important as doctors need information of "absolute" BP in DBPs and SBPs for diagnosis. This "absolute" BP is defined as those at the arterial outlet from the heart, i.e., aorta. Due to this, all the qualified non-invasive BP measurement devices available in the market need to be carefully calibrated before usage to accurately predict the "absolute" BP in DBP and SBP, actually correlating well to BPs at heart outlet, based on measurements elsewhere. These calibrations are conducted via non-theoretical based low- or high-order interpolations. Moderate inaccuracy results are expected, mostly resulted from lack of theoretical basis for these interpolations. With BPTT established and its computation algorithm developed, higher accuracy by less calibration times are expected.

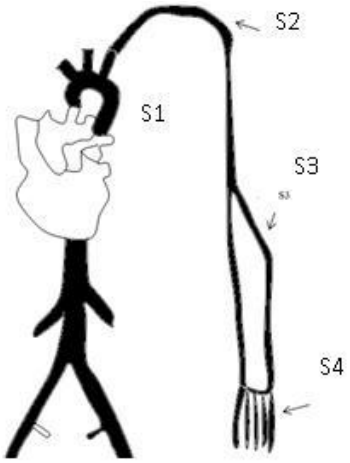

Fig. 5. Upper extremity vessels of the cardiovascular system.

The development for the algorithm for BPTT is started with considering the upper extremity vessels the cardiovascular system as shown in Fig. 5, where sections S1 to S4 are, respectively, aorta, major artery, small artery, and periphery [13], which correspond human body locations of to heart outlet, upper arm, forearm and fingertips, respectively. Based on the BPTT developed in Eq. (8), PPG signals measured at S4 (fingertips) can be used to render accurate BPs at S1 (aorta), which is desired by doctors for effective diagnosis. In this duty, however, due to great difficulty to obtain realistic data of BPs at aorta, the development of the algorithm is practiced for predicting BPs at S2 (forearm) based on the PPG signals measured at S4 (fingertips). In parallel with the measured PPGs at S4, the BP at S2 is also measured by a validated commercial BP device. Once the computation algorithm is developed for predicting BPs at S2 based on S4, the parameters are calibrated by commercial data at S2 and then the performance of BPTT is evaluated based on the comparison of the BPs predicted by the algorithm to commercial data.

The development of the algorithm is started with adopting the results in the work [15], which stated that the frequency of the main component of SBP and DBP waveforms in the upper arm, forearm and fingers (S2, S3 and S4, respectively) are approximately four times of heart rate, i.e., $4\omega_b$. Thus, according to Eq. (8), the relationship between the blood pressure waveform $P(z_3, t)$ at S3 location and the blood pressure waveform $P(z_4,t)$ at S4 location can be characterized by

$$P(z_4, t) \approx P(z_3, t)\,[a_{43}\cos(4\omega t) + (1 - a_{43})], \qquad (12)$$

where a_{43} denotes the strength coefficient of systole and diastole as transport from S3 to S4. The relationship of blood pressure waveforms between S2 and S3 is similar to the above, i.e.,

$$P(z_3, t) \approx P(z_2, t)\,[a_{32}\cos(4\omega t) + (1 - a_{32})], \qquad (13)$$

where a_{32} denotes the strength coefficient of systole and diastole as transport from S3 to S4. Combining Eqs. (12) and (13), the relation between the blood pressure waveforms at S2 and S4 can be obtained as below,

$$P(z_4, t) = P(z_2, t)[a_{32}\cos(4\omega t) + (1 - a_{32})][a_{43}\cos(4\omega t) + (1 - a_{43})]. \qquad (14)$$

From Eq. (7), $P(z_2, t)$ and $P(z_4, t)$ can be expressed as a series combination of harmonics based on heart rate, that is,

$$P(z_2, t) = P_{2,0} + P_{2,1}\cos\omega t + P_{2,2}\cos 2\omega t + P_{2,3}\cos 3\omega t + P_{2,4}\cos 4\omega t + P_{2,5}\cos 5\omega t + P_{2,6}\cos 6\omega t + \cdots, \qquad (15a)$$

$$P(z_4, t) = P_{4,0} + P_{4,1}\cos\omega t + P_{4,2}\cos 2\omega t + P_{4,3}\cos 3\omega t + P_{4,4}\cos 4\omega t + P_{4,5}\cos 5\omega t + P_{4,6}\cos 6\omega t + \cdots. \qquad (15b)$$

Substituting the expressions in Eqs. (15) into (14), expanding all harmonics at both sides of the equation and then performing the well-known harmonic balancing for first- and second-order harmonics yield $P_{4,1}$ and $P_{4,2}$, as belows,

$$P_{4,1} = P_{2,1}(1 - a_{43})(1 - a_{32}) + P_{2,1}\frac{a_{43}a_{32}}{2} + (P_{2,3} + P_{2,5})[\frac{a_{43}}{2}(1 - a_{32}) + \frac{a_{32}}{2}(1 - a_{43})], \qquad (16)$$

$$P_{4,2} = P_{2,2}(1 - a_{43})(1 - a_{32}) + P_{2,2}\frac{a_{43}a_{32}}{2} + (P_{2,2} + P_{2,6})[\frac{a_{43}}{2}(1 - a_{32}) + \frac{a_{32}}{2}(1 - a_{43})]. \qquad (17)$$

The equation used for harmonic balancing that leads to Eqs. (16), (17) is given in Appendix. In theory, the strength coefficients of a_{32} and a_{43} can be solved via Eqs. (16), (17) based on calibrations and Fourier transforms on $P(z_3, t)$ and $P(z_3, t)$. Then $P_{2,1}$ and $P_{2,2}$ are solved subsequently based on Eqs. (16), (17). With solved $P_{2,1}$ and $P_{2,2}$, higher-order components associated with the blood pressures at S2 can then be also found, able to predict SBPs, DBPs and PPs at S2.

Aiming for less computation load for the CPU in a smart phone, i.e., no Fourier Transforms and solving nonlinear algebraic equations (17), approximations are further assumed to simplify the computation process of predicting SBPs and DBPs at S2 based on S4, which is started with recognizing the aforementioned fact as illustrated by Fig. 2 that SBP is the summation of PP and DBP. The main oscillatory component of the blood pressure is in the frequency of heart beat (HB), which is characterized mainly by pulse pressure (PP), following the method presented in this study. Since the HB components in the formulation (15a) are captured by $P_{2,1}$, the PP at S2 to predict can be assumed as

$$PP_2 = c_{1,PP}P_{2,1} + c_{0,PP}, \qquad (18)$$

where $c_{1,\mathrm{PP}}$ and $c_{0,\mathrm{PP}}$ are interpolation parameters. Noting that all a's are in small values, thus, $P_{2,1} \approx P_{4,1}$ based on Eq. (16), then, Eq. (18) becomes

$$PP_2 = c_{1,PP}P_{4,1} + c_{0,PP}. \qquad (19)$$

Having effective calibration to identify $c_{1,\mathrm{PP}}$ and $c_{0,\mathrm{PP}}$, Eq. (19) is ready to be used for predicting pulse pressure (PP) at S2 based on the magnitude of the first-order harmonic at HR measured at S4.

With PPs obtained at desired location, efforts are next paid to predict diastolic blood pressures (DBPs) at S2 based on S4. Based on the characterization of blood pressure waveforms as illustrated in Fig. 2, SBP can be calculated by summing DBP and PP. To solve for DBP, the harmonic balancing on Eq. (A1) for zero- and fourth-order harmonics at both sides yields

$$P_{4,0} = P_{2,0}(1-a_{43})(1-a_{32}) + P_{2,0}\frac{a_{43}a_{32}}{2} + \frac{P_{2,4}}{2}[a_{43}(1-a_{32}) + a_{32}(1-a_{43})], \quad (20a)$$

$$P_{4,4} = P_{2,4}(1-a_{43})(1-a_{32}) + P_{2,4}\frac{3a_{43}a_{32}}{4} + P_{2,0}[a_{43}(1-a_{32}) + a_{32}(1-a_{43})]. \quad (20b)$$

The above two equations reveals that the zero- and fourth-order harmonics at S2, $P_{2,0}$ and $P_{2,4}$, are both linear combinations of $P_{4,0}$ and $P_{4,4}$. On the other hand, based on the definition of DBP as illustrated by Fig. 2 is the constant (dc) part of the blood pressure waveform, that is, proportional to $P_{2,0}$; therefore, the DBP at S2 to be predicted by measured waveforms at S4 can be formulated by

$$DBP_2 = c_{1,DBP}P_{4,0} + c_{2,DBP}P_{4,4} + c_{0,DBP}. \quad (21)$$

Finally, SBP at S2 is the sum of DBP and PP, yielding

$$SBP_2 = DBP_2 + PP_2. \quad (22)$$

With Eqs. (19), (21) and (22) in hands, one is able to predict SBP and DBP at forearm (S2) by measured PPG waveforms at fingertips (S4) and properly-calibrated parameters, $c_{1,DBP}$, $c_{2,DBP}$, $c_{0,DBP}$, $c_{1,PP}$ and $c_{0,PP}$. The characteristics of the measurements at S4 required for BP predictions at S2 are zero-, first- and fourth-order harmonics. These harmonics can be extracted effectively and efficiently by utilizing appropriate band-pass filters at designated frequencies. Finally, it is pertinent to note herein that the characteristics of the established Eqs. (19), (21) and (22) complies with those reported by [15] which found zero-, first- and fourth-order harmonics at the ends of cardiovascular branches affects the waveforms measured at front parts of the human arterial system, including forearm. In theory, this is due to nonlinear harmonic reflection at the extremities of arterial vessels and branches. Also found is that when the energy of the 4th harmonic of the blood pressure waveform, $P_{4,4}$, decreases, the dc part of the blood pressure waveform, $P_{4,0}$, increased, coinciding with the fact that the values of $c_{2,DBP}$ identified later in experiments are often negative, opposite to that of $c_{1,DBP}$.

III. Experimental Validation

With BPTT and algorithm developed, an experimental platform with multiple physiological diagnosis functions is built for regional blood pressure detections and ensuing computations based on the algorithm. The proposed platform consists of two parts: (1) the peripheral kernel with Altera Nios II embedded system and (2) the PPG analysis kernel. The key idea herein is to design for a quick verification prototype on a portable system, like a mobile smart phone. The physiological signal detection device can then be easily added with the peripheral kernel. The overview of this platform is shown in Fig. 6. The peripheral kernel is established by Nios II embedded system with 100-MHz clock rate on the DE2 Design Kit. The kernel is proposed to serve as a peripheral interface manager. All of the peripheral interface, like the keypad, SDRAM, flash, audio CODEC, SD Card, RS-232, LCM, the HRV and PPG analysis kernel are controlled by this kernel as shown in Fig. 7.

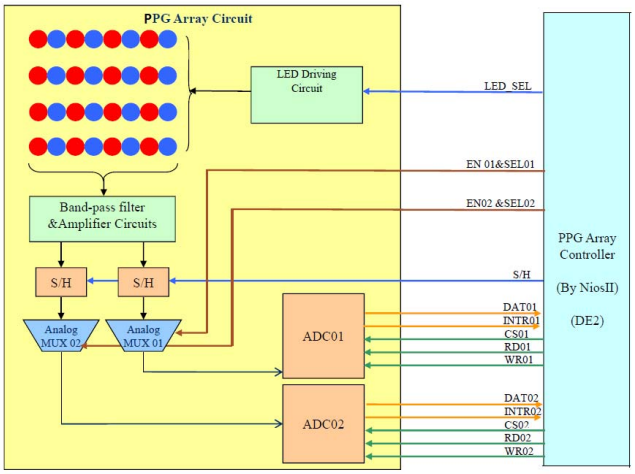

Fig. 6. Functional blocks of proposed sensor system.

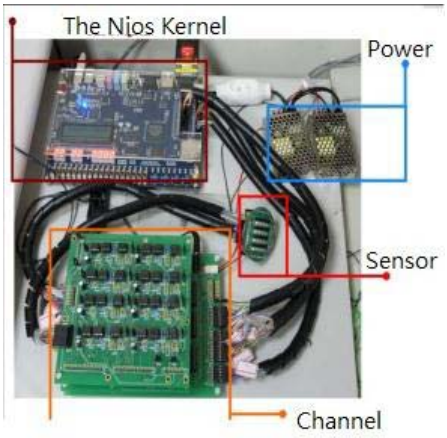

Fig. 7. The experiment platform.

Experiments were conducted for 5 healthy subjects aged between 20 and 24 years old. The environment of this experiment was in a room at temperature about 25 °C. The tests for stability of the sensor and algorithm is performed. Prior to the stability test for each subject, calibration was performed to obtained parameter values of $c_{1,DBP}$, $c_{2,DBP}$, $c_{0,DBP}$, $c_{1,PP}$ and $c_{0,PP}$. For example, for subject 1, the identified values of $c_{1,DBP}$, $c_{2,DBP}$, $c_{0,DBP}$, $c_{1,PP}$ and $c_{0,PP}$ are (8.72, 134.56, 83.71, 9.34, 6.28), respectively. With all c's identified, the sensor platform was operated to predict SBPs, DBPs and PPs at forearm based on the blood pressure waveforms in PPGs sensed at fingertips. The results are summarized in Table. I, where it is seen that for each subject, two-time measurements are taken for evaluating the stability of the sensor system, the error percentage of predicted SBPs and

TABLE I
STABILITY TEST RESULTS

	NO. of objects	1	2	3	4	5
First time	SBP	131	126	107	122	114
	DBP	83	80	63	81	70
	Heart Rate	77	98	74	104	77
Second time	SBP	130	125	113	124	117
	DBP	79	79	68	85	73
	Heart Rate	79	97	71	98	73
Error	SBP	1%	1%	5%	4%	3%
	DBP	3%	1%	6%	5%	4%
	Heart Rate	2%	1%	3%	6%	5%

TABLE II
THE MEASUREMENTS COMPARED TO OMRON'S COUNTERPARTS

NO.	This sensor			Omron		
	SBP	DBP	Heart Rate	SBP	DBP	Heart Rate
1	125	82	80	125	87	88
2	128	86	94	133	85	90
3	121	77	83	131	79	89
4	120	63	65	119	74	62
5	131	81	74	115	73	69
6	113	68	83	122	74	82
7	121	75	74	120	76	74
8	126	75	68	108	72	66
9	104	58	53	102	57	55
10	122	80	82	116	69	77
11	114	62	62	109	68	64
12	112	68	68	104	57	66
13	114	80	79	116	68	79
14	132	77	61	117	80	63
15	107	74	72	126	83	77
16	126	82	80	121	88	83
17	125	76	71	121	84	77
18	123	76	74	119	78	73
19	130	91	104	131	87	107
20	125	86	94	124	84	99
21	127	85	89	126	90	87
22	121	77	82	123	84	83
23	124	85	86	124	90	86
24	128	87	103	130	86	101
25	124	82	94	128	85	94
26	123	77	88	129	83	84
27	120	76	76	114	82	73
28	127	78	79	123	78	79
29	134	92	86	127	92	90
30	119	76	82	122	81	78

DBPs to their corresponding averages were controlled under 6%, a satisfactory performance.

With stability satisfied, experiments were conducted with 30 healthy subjects aged between 21 and 27 years old

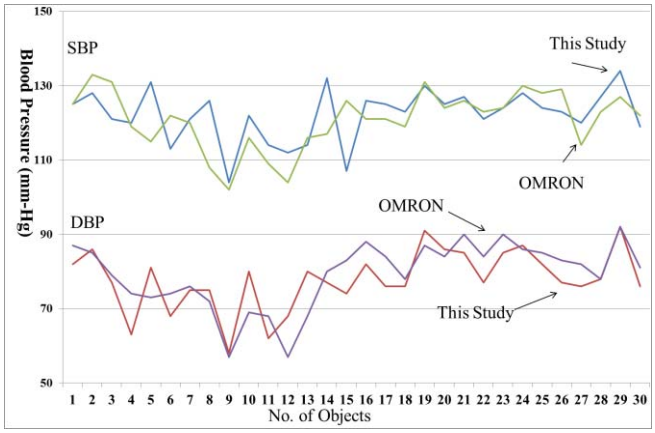

Fig. 8. Comparison of blood pressures.

(a) (b)

Fig. 9. The proposed image sensor implemented in a smart phone: (a) measuring and (b) measured BP waveforms and calculated SBPs, DBPs and HRs.

(average age of 22.19 years old while standard deviation of 1.5 years). The environment of this experiment was in a room at temperature about 25 ± 2 °C. The measurements are compared to Omron sphygmomanometer for different people, which are listed in Table. II. The results listed in Table II are also illustrated by Fig. 8. Seen from the obtained experimental data given in Table II, the average on the differences between the SBPs sensed by the proposed sensor and Omron's is 1.37 mmHg, while for DBPs is −1.40 mmHg. The standard deviations are 7.61 (mmHg) and 6.00 (mmHg) for SBPs and DBPs, respectively. The afore-reported averages and standard deviations are well below those required by the Association for the Advancement of Medical Instrumentation (AAMI), which are ±5 mmHg and 8 mmHg, respectively, for SBPs and DBPs. The successfully-developed algorithm is implemented in a smart phone with a designed user interface, as shown in Fig. 9.

IV. DISCUSSION

Blood pressures in systole and diastole are successfully measured by a newly-established blood pressure transport theory (BPTT) and its ensuing computation algorithm. With the algorithm, the developed sensor system can be easily calibrated and then used for predicting systolic and diastolic blood pressures (SBPs and DBPs) based on PPG signals that can be sensed by a portable device, like a CMOS image camera in a smart phone, further paving the way for ubiquitous blood

pressure sensing. The sensor and methodology presented in this study lead to satisfactory levels of accuracy in predicting SBPs and DBPs as compared to the standards set by the Association for the Advancement of Medical Instrumentation. Future efforts will be dedicated to improve the proposed methodology for long-range sensing such that ubiquitous and convenient blood pressure sensing becomes possible and set the bases for diagnosis.

APPENDIX

The harmonic balancing is performed based on the equalization of the respective harmonics between the series expansion of the PPG blood pressure waveforms captured at fingertips (S4) and forearm (S2), that is based on

$$\begin{aligned}
&P(z4,t)\\
&= P_{4,0} + P_{4,1}\cos\omega t + P_{4,2}\cos 2\omega t\\
&\quad + P_{4,3}\cos 3\omega t + P_{4,4}\cos 4\omega t + \cdots\\
&= [P_{2,0}(1-a_{32})(1-a_{43}) + P_{2,4}\frac{a_{32}}{2}(1-a_{43})\\
&\quad + P_{2,4}\frac{a_{43}}{2}(1-a_{32}) + \frac{P_{2,0}}{2}a_{32}a_{43}]\\
&\quad + [P_{2,1}(1-a_{32})(1-a_{43}) + P_{2,3}\frac{a_{32}}{2}(1-a_{43})\\
&\quad + P_{2,3}\frac{a_{43}}{2}(1-a_{32}) + P_{2,5}\frac{a_{32}}{2}(1-a_{43})\\
&\quad + P_{2,5}\frac{a_{43}}{2}(1-a_{32}) + \frac{P_{2,1}}{2}a_{32}a_{43}]\cos\omega t\\
&\quad + [P_{2,2}(1-a_{32})(1-a_{43}) + P_{2,2}\frac{a_{32}}{2}(1-a_{43})\\
&\quad + P_{2,2}\frac{a_{43}}{2}(1-a_{32}) + P_{2,6}\frac{a_{32}}{2}(1-a_{43})\\
&\quad + P_{2,6}\frac{a_{43}}{2}(1-a_{32}) + \frac{P_{2,2}}{2}a_{32}a_{43}]\cos 2\omega t\\
&\quad + [P_{2,3}(1-a_{32})(1-a_{43}) + P_{2,1}\frac{a_{32}}{2}(1-a_{43})\\
&\quad + P_{2,1}\frac{a_{43}}{2}(1-a_{32}) + \frac{P_{2,3}}{2}a_{32}a_{43}]\cos 3\omega t\\
&\quad + [P_{2,4}(1-a_{32})(1-a_{43}) + P_{2,0}a_{32}(1-a_{43})\\
&\quad + P_{2,0}a_{43}(1-a_{32}) + \frac{3}{4}P_{2,4}a_{32}a_{43}]\cos 4\omega t\\
&\quad + \cdots .
\end{aligned}$$

REFERENCES

[1] D. Zito *et al.*, "Wearable system-on-a-chip UWB radar for contact-less cardiopulmonary monitoring: Present status," in *Proc. EMBS*, Aug. 2008, pp. 5274–5277.

[2] D. Girbau, A. M. Roldan, A. Ramos, and R. Villarino, "Remote sensing of vital signs using a doppler radar and diversity to overcome null detection," *IEEE Sensors J.*, vol. 12, no. 3, pp. 512–518, Mar. 2012.

[3] R. Sokwoo, B.-H. Yang, and H. H. Asada, "Artifact-resistant power-efficient design of finger-ring plethysmographic sensors," *IEEE Trans. Biomed. Eng.*, vol. 48, no. 7, pp. 795–805, Jul. 2001.

[4] C. Lee, H. S. Shin, J. Park, and J.-H. Lee, "The optimal attachment position for a fingertip photoplethysmographic sensor with low DC," *IEEE Sensors J.*, vol. 12, no. 5, pp. 1253–1254, May 2012.

[5] M. R. Ram, K. V. Madhav, E. H. Krishna, N. R. Komalla, and K. A. Reddy, "A novel approach for motion artifact reduction in PPG signals based on AS-LMS adaptive filter," *IEEE Trans. Instrum. Meas.*, vol. 61, no. 5, pp. 1445–1457, May 2012.

[6] T.-Y. Tu, P. C.-P. Chao, and Y.-P. Lee, "A new non-invasive cuff-less blood pressure sensor," in *Proc. IEEE Sensors Conf.*, Nov. 2013, pp. 1–4.

[7] Y.-Y. L. Wang, C. C. Chang, J. C. Chen, H. Hsiu, and W. K. Wang, "Pressure wave propagation in arteries. A model with radial dilatation for simulating the behavior of a real artery," *IEEE Eng. Med. Biol. Mag.*, vol. 16, no. 1, pp. 51–54, Jan./Feb. 1997.

[8] Y.-Y. L. Wang, M.-Y. Jan, C.-S. Shyu, C.-A. Chiang, and W.-K. Wang, "The natural frequencies of the arterial system and their relation to the heart rate," *IEEE Trans. Biomed. Eng.*, vol. 51, no. 1, pp. 193–195, Jan. 2004.

[9] Y.-Y. L. Wang *et al.*, "The ventricular-arterial coupling system can be analyzed by the eigenwave modes of the whole arterial system," *Appl. Phys. Lett.*, vol. 92, no. 15, pp. 153901-1–153901-3, Apr. 2008.

[10] Y.-Y. L. Wang, W.-B. Chiu, M.-Y. Jan, J.-G. Bau, S.-P. Li, and W.-K. Wang, "Analysis of transverse wave as a propagation mode for the pressure pulse in large arteries," *J. Appl. Phys.*, vol. 102, no. 6, pp. 064702-1–064702-4, Sep. 2007.

[11] Y. Y. Wang, S. L. Chang, Y. E. Wu, T. L. Hsu, and W. K. Wang, "Resonance. The missing phenomenon in hemodynamics," *Circulat. Res.*, vol. 69, no. 1, pp. 246–249, 1991.

[12] H. Hsiu, P.-T. Chao, T.-L. Hsu, and W.-K. Wang, "Effects of weak external mechanical force stimulation on the heart rate variability of rats," *Biomed. Eng., Appl., Basis Commun.*, vol. 16, no. 6, pp. 313–321, Dec. 2004.

[13] K. Chellappan, E. Zahedi, and M. A. M. Ali, "Age-related upper limb vascular system windkessel model using photoplethysmography," in *Proc. 3rd Kuala Lumpur Int. Conf. Biomed. Eng.*, Dec. 2006, pp. 563–566.

[14] H. Hsiu, C. L. Hsu, C. T. Chen, W. C. Hsu, H. F. Hu, and F. C. Chen, "Correlation of harmonic components between the blood pressure and photoplethysmography waveforms following local-heating stimulation," *Int. J. Biosci., Biochem. Bioinform.*, vol. 2, no. 4, pp. 248–253, Jul. 2012.

[15] S.-H. Wang, W.-K. Wang, T.-L. Hsu, M.-Y. Jan, and Y.-Y. L. Wang, "Effects of captopril on specific harmonic indexes of the peripheral pressure pulse waveform," in *Proc. 4th Int. Conf. Bioinform. Biomed. Eng.*, Jun. 2010, pp. 1–3.

[16] M.-Z. Poh, D. J. McDuff, and R. W. Picard, "Non-contact, automated cardiac pulse measurements using video imaging and blind source separation," *Opt. Exp.*, vol. 18, no. 10, pp. 10762–10774, May 2010.

[17] B. Tursky, D. Shapiro, and G. E. Schwartz, "Automated constant cuff-pressure system to measure average systolic and diastolic blood pressure in man," *IEEE Trans. Biomed. Eng.*, vol. 19, no. 4, pp. 271–276, Jul. 1972.

[18] S. Haykin, *Communication Systems*. New York, NY, USA: Wiley, 2001.

Sheng-Chieh Huang was born in Chunghua, Taiwan, in 1967. He is currently an Assistant Professor with the Department of Electrical and Computer Engineering, National Chiao Tung University, Hsinchu, Taiwan.

Pei-Hsuan Hung was born in Kaohsiung, Taiwan, in 1992. He received the B.S. degree in electrical and computer engineering from National Chiao Tung University, Hsinchu, Taiwan. He is currently pursuing the M.S. degree at the Graduate Institute of Communication Engineering, National Taiwan University, Taipei, Taiwan. His major research interests include biosignal processing, image processing, and algorithmic composition.

Chung-Hung Hong was born in Kaohsiung, China. He received the B.S. degree in electrical and computer engineering from National Chiao Tung University, Hsinchu, Taiwan, in 2012. His major research interests include linear control, RF IC design, and blood circulation dynamics.

Hui-Min Wang was born in Tainan, Taiwan, in 1969. He received the B.S. and M.S. degrees in mathematics from Chung Yuan Christian University, Taoyuan, Taiwan, in 1993 and 1995, respectively. He is currently pursuing the Ph.D. degree at the Graduate Institute of Electrical Control Engineering, National Chiao Tung University, Hsinchu, Taiwan. His major research interests include music physiology, algorithmic composition, and computational aesthetics.